Available online at www.sciencedirect.com
ScienceDirect
Biochimica et Biophysica Acta 1768 (2007) 2130–2144
Biochimica et Biophysica Acta BBA
www.elsevier.com/locate/bbamem

Dynamics and heterogeneity of bovine hippocampal membranes: Role of cholesterol and proteins

Soumi Mukherjee [a], Mamata Kombrabail [b], G. Krishnamoorthy [b,*], Amitabha Chattopadhyay [a,*]

[a] *Centre for Cellular and Molecular Biology, Uppal Road, Hyderabad 500 007, India*
[b] *Department of Chemical Sciences, Tata Institute of Fundamental Research, Homi Bhabha Road, Mumbai 400 005, India*

Received 5 December 2006; received in revised form 5 May 2007; accepted 29 May 2007
Available online 2 June 2007

Abstract

The structural and dynamic consequence of alterations in membrane lipid composition (specifically cholesterol) in neuronal membranes is poorly understood. Previous work from our laboratory has established bovine hippocampal membranes as a convenient natural source for studying neuronal receptors. In this paper, we have explored the role of cholesterol and proteins in the dynamics and heterogeneity of bovine hippocampal membranes using fluorescence lifetime distribution analysis of the environment-sensitive fluorescent probe Nile Red incorporated into such membranes by the maximum entropy method (MEM), and time-resolved fluorescence anisotropy measurements. The peak position and the width of the lifetime distribution of Nile Red show a progressive reduction with increasing cholesterol depletion from native hippocampal membranes indicating that the extent of heterogeneity decreases with decrease in membrane cholesterol content. This is accompanied by a concomitant decrease of the fluorescence anisotropy and rotational correlation time. Our results point out that the microenvironment experienced by Nile Red is relatively insensitive to the presence of proteins in hippocampal membranes. Interestingly, Nile Red lifetime distribution in liposomes of lipid extracts is similar to that of native membranes indicating that proteins do not contribute significantly to the high level of heterogeneity observed in native membranes. These results could be relevant in understanding the neuronal diseases characterized by defective membrane lipid metabolism.

Keywords: Hippocampal membrane; Cholesterol; Fluorescence lifetime distribution; Maximum entropy method; Time-resolved fluorescence anisotropy

1. Introduction

The nervous system characteristically contains a very high concentration of lipids, and displays remarkable lipid diversity [1]. The lipid composition of cells that make up the nervous system is unique and has been correlated with increased complexity in the organization of the nervous system during evolution [2]. Organization and dynamics of cellular membranes in the nervous system play a crucial role in the function of neuronal membrane receptors. Cholesterol is an important lipid in this context since it is known to regulate the function of neuronal receptors [3,4] thereby affecting neurotransmission and giving rise to mood and anxiety disorders [5]. Interestingly, the central nervous system which accounts for only 2% of the body mass contains ~25% of free cholesterol present in the whole body [6]. Although the brain is highly enriched in cholesterol, the organization and dynamics of brain cholesterol is still poorly understood [7]. Brain cholesterol is synthesized *in situ* [8] and is developmentally regulated [9]. The organization, traffic, and dynamics of brain cholesterol are stringently controlled since the input of cholesterol into the central nervous system is almost exclusively from *in situ* synthesis as there is no evidence for the transfer of cholesterol from blood plasma to brain [6]. As a result, a number of neurological diseases share a common etiology of defective cholesterol metabolism in the

Abbreviations: BCA, Bicinchoninic acid; DMPC, 1,2-dimyristoyl-*sn*-glycero-3-phosphocholine; DOPC, dioleoyl-*sn*-glycero-3-phosphocholine; FWHM, full width at half maximum; MβCD, methyl-β-cyclodextrin; MEM, maximum entropy method; MLV, multilamellar vesicle; Nile Red, 9-diethylamino-5H-benzo[α]phenoxazine-5-one; PMSF, phenylmethylsulfonyl fluoride; TCSPC, time correlated single photon counting

* Corresponding authors. G. Krishnamoorthy is to contacted at Department of Chemical Sciences, Tata Institute of Fundamental Research, Homi Bhabha Road, Mumbai 400 005, India. Tel.: +91 22 2278 2301; fax: +91 22 2280 4610. A. Chattopadhyay, Centre for Cellular and Molecular Biology, Uppal Road, Hyderabad 500 007, India. Tel.: +91 40 2719 2578; fax: +91 40 2716 0311.

E-mail addresses: gk@tifr.res.in (G. Krishnamoorthy), amit@ccmb.res.in (A. Chattopadhyay).

0005-2736/$ - see front matter © 2007 Elsevier B.V. All rights reserved.
doi:10.1016/j.bbamem.2007.05.025

brain [6,10]. In addition, several epidemiological studies indicate a possible role of lipids in a variety of neurological disorders which have been shown to involve deregulated lipid metabolism [1,10]. Yet, the organization and dynamics of neuronal membranes as a consequence of alterations in membrane lipid composition (specifically cholesterol) is poorly understood [7]. In view of the importance of cholesterol in relation to membrane domains [11–15], the effect of alteration in the cholesterol content of neuronal membranes on membrane dynamics and protein/receptor function represents an important determinant in the analysis of neurogenesis and several neuropathologies.

Previous work from our laboratory has established native membranes prepared from the bovine hippocampus as a convenient natural source for studying the serotonin$_{1A}$ (5-HT$_{1A}$) receptor which is an important member of the seven transmembrane domain G-protein coupled receptor family [16]. We have partially purified and solubilized the 5-HT$_{1A}$ receptor from bovine hippocampus in a functionally active form [17]. Interestingly, we have recently shown the requirement of membrane cholesterol in modulating ligand binding activity of the 5-HT$_{1A}$ receptor using a number of approaches [4,18]. In order to correlate these cholesterol-dependent functional changes with changes in membrane organization and dynamics, we have previously utilized Laurdan generalized polarization [19], and wavelength-selective fluorescence [20] approaches to examine the membrane microenvironment and its modulation with cholesterol and protein content.

Cell membranes could be considered as anisotropic, two-dimensional fluid with characteristic dynamics [21]. Considerable evidence shows that the biological membrane exhibits lateral heterogeneity in composition of membrane components and physical properties such as order. The static picture of cell membranes visualized as barriers enclosing various cellular compartments is currently being replaced by a dynamic and heterogeneous description. The heterogeneity could be manifested as both spatial and temporal domains [22]. Interestingly, cholesterol has been previously reported to influence membrane heterogeneity [13,22,23]. Due to their dynamic nature, spectroscopic techniques are conveniently used for monitoring membrane heterogeneity. Fluorescence spectroscopy is extensively used for this purpose due to its intrinsic sensitivity, suitable time scale, and minimum perturbation [24,25]. In this paper, we have explored the role of cholesterol and proteins in the dynamics and heterogeneity of bovine hippocampal membranes using fluorescence lifetime distribution analysis of Nile Red incorporated into such membranes by the maximum entropy method (MEM), and time-resolved fluorescence anisotropy measurements. Nile Red (9-diethylamino-5H-benzo[α]phenoxazine-5-one), is an uncharged phenoxazone dye, whose fluorescence properties are altered by the polarity of its immediate environment due to a large change in dipole moment upon excitation [26–28]. This large change in dipole moment has been attributed to charge separation between the diethylamino group which acts as the electron donor and the quinoid part of the molecule which serves as the electron acceptor.

2. Materials and methods

2.1. Materials

Cholesterol, MβCD, DMPC, EDTA, EGTA, iodoacetamide, PMSF, sucrose, polyethylenimine, sodium azide, Na_2HPO_4, Nile Red, Tris and MOPS were obtained from Sigma Chemical Co. (St. Louis, MO). BCA reagent kit for protein estimation was from Pierce (Rockford, IL). Amplex Red cholesterol assay kit was from Molecular Probes (Eugene, OR). Concentrations of stock solution of Nile Red in methanol were estimated using the molar extinction coefficient (ε) of 45,000 M^{-1} cm^{-1} at 552 nm [29]. All other chemicals used were of the highest purity available. Solvents used were of spectroscopic grade. Water was purified through a Millipore (Bedford, MA) Milli-Q system and used throughout. Fresh bovine brains were obtained from a local slaughterhouse within 10 min of death and the hippocampal region was carefully dissected out. The hippocampi were immediately flash frozen in liquid nitrogen and stored at −70 °C till further use.

2.2. Methods

2.2.1. Preparation of native hippocampal membranes

Native hippocampal membranes were prepared as described previously [19]. Native membranes were suspended in a minimum volume of 50 mM Tris, pH 7.4 buffer, homogenized using a hand-held Dounce homogenizer, flash frozen in liquid nitrogen and stored at −70 °C. Protein concentration was assayed using the BCA reagent with bovine serum albumin as standard [30]. The phospholipid content of these membranes is typically ~960 nmol/mg of total protein [31].

2.2.2. Cholesterol depletion of native membranes

Native hippocampal membranes were depleted of cholesterol using MβCD as described previously [18,31]. Briefly, membranes with a total protein concentration of 2 mg/ml were treated with different concentrations of MβCD in 10 mM MOPS buffer (pH 7.4) at 25 °C in a temperature controlled water bath with constant shaking for 1 h. Membranes were then spun down at 50,000×*g* for 5 min, washed once with MOPS buffer and resuspended in the same buffer. Cholesterol was estimated using the Amplex Red cholesterol assay kit [32].

2.2.3. Lipid extraction from native and cholesterol-depleted membranes

Lipid extraction was carried out according to the method of Bligh and Dyer [33] from native hippocampal membranes. The lipid extract was finally resuspended in a mixture of chloroform–methanol (1:1, v/v).

2.2.4. Estimation of inorganic phosphate

Concentration of lipid phosphate was determined subsequent to total digestion by perchloric acid [34] using Na_2HPO_4 as standard. DMPC was used as an internal standard to assess lipid digestion. Samples without perchloric acid digestion produced negligible readings.

2.2.5. Sample preparation

Membranes (native and cholesterol-depleted) containing 100 nmol of total phospholipid were suspended in 2 ml of 10 mM MOPS buffer (pH 7.4). The amount of Nile Red added from a methanolic stock solution was such that the final fluorophore concentration was 0.2 mol% (1 mol% for steady state fluorescence measurements) with respect to the total phospholipid content. The resultant probe concentration was 0.1 μM (0.5 μM for steady state fluorescence measurements) in all cases and the methanol content was always low (0.02–0.09%, v/v). This ensures optimal fluorescence intensity with negligible membrane perturbation. Nile Red was added to membranes while being vortexed for 1 min at room temperature (~25 °C) and kept in the dark for 1 h before measurements. Background samples were prepared the same way except that Nile Red was omitted. The protein concentration was ~0.04 mg/ml.

Lipid extracts containing 100 nmol of total phospholipid in chloroform–methanol (1:1, v/v) were mixed well with 1 nmol of Nile Red in methanol. The sample was mixed well and dried under a stream of nitrogen while being warmed gently (~45 °C). After further drying under a high vacuum for at least 6 h, 2 ml of 10 mM MOPS, pH 7.4 buffer was added and lipid samples were hydrated (swelled) at ~70 °C while being intermittently vortexed for 3 min to disperse the lipid and form homogeneous multilamellar vesicles (MLVs). The

MLVs were kept at ~70 °C for an additional hour to ensure proper swelling as the vesicles were formed. Such high temperatures were necessary for hydrating the samples due to the presence of lipids with high melting temperature in neuronal tissues [35]. Samples were kept in the dark at room temperature (~25 °C) overnight before taking fluorescence measurements. MOPS buffer was used to avoid any change in pH due to temperature change since the change in pK_a/°C for MOPS is negligible (−0.006) [36].

2.2.6. Steady state fluorescence measurements

Steady state fluorescence measurements with Nile Red were performed with a Hitachi F-4010 steady state spectrofluorometer equipped with a stirring accessory and thermostated (±0.1 °C) by a circulating water bath, using 1 cm path length quartz cuvettes. While heating, the sample temperature was continuously measured with a thermocouple. Excitation and emission slits with nominal bandpass of 5 nm were used for all measurements. Background intensities of samples in which the fluorophore was omitted were negligible in most cases and were subtracted from each sample spectrum to cancel out any contribution due to the solvent Raman peak and other scattering artifacts. Steady state fluorescence anisotropy measurements were performed using a Hitachi polarization accessory. Anisotropy values were calculated from the equation [37]:

$$r = \frac{I_{VV} - \mathbf{G}I_{VH}}{I_{VV} + 2\mathbf{G}I_{VH}} \quad (1)$$

where I_{VV} and I_{VH} are the measured fluorescence intensities (after appropriate background subtraction) with the excitation polarizer vertically oriented and emission polarizer vertically and horizontally oriented, respectively. **G** is the grating correction factor and is the ratio of the efficiencies of the detection system for vertically and horizontally polarized light, and is equal to I_{HV}/I_{HH}. All experiments were done with multiple sets of samples and average values of anisotropy are shown in Figs. 4c and 8a.

2.2.7. Time-resolved fluorescence measurements

Time-resolved fluorescence decays were obtained by time correlated single photon counting (TCSPC) setup coupled to a picosecond laser. The exciting laser source was a cavity dumped, mode-locked, picosecond Rhodamine 6G dye laser (570–630 nm) (Spectra Physics) synchronously pumped by the frequency doubled (532 nm, 400–600 mW) output of CW, mode-locked Nd-YAG laser (Spectra Physics series 3000). A pulse repetition rate of 82 MHz was reduced to a repetition rate of 800 kHz by cavity dumping (in the Rhodamine 6G dye laser). The dye was continuously circulated to avoid any photobleaching. The pulse width of the excitation laser beam was typically 4–10 ps, and the average power was typically between 15 and 30 mW. The fundamental wavelengths of the Rhodamine 6G dye laser used for exciting the fluorophores are within 570–630 nm. Samples were excited at 575 nm. Since the pulse repetition rate of the laser pulses was 800 kHz, the fluorescence photons were collected at the count rate of <8000 counts/s. The instrument response function (IRF) was measured using a scattering solution of dilute non-dairy creamer in water. Non-dairy creamer in water is a suspension of fine particles without any fluorescence and we have also found a very similar IRF with other non-fluorescence suspensions. The Full Width at Half Maximum (FWHM) of the IRF was typically ~40 ps.

The samples were thermostated (±0.1 °C) by a circulating water bath in 1 cm path length quartz cuvettes. While heating, the sample temperature was continuously measured with a thermocouple. For the measurement of fluorescence lifetimes, fluorescence decay was collected from the sample after excitation with the emission polarizer oriented at the magic angle (54.7°) with respect to the excitation polarizer. The fluorescence decay collected at the magic angle represents the total fluorescence intensity decay because of the absence of any anisotropic components in the fluorescence decay at this particular angle. The fluorescence emission at magic angle (54.7°) was dispersed in a monochromator (spectral width 2.5 nm) and counted ($3–4\times10^3$ s^{-1}) by a microchannel plate photomultiplier, and processed through constant fraction discriminator, time-to-amplitude converter and multichannel analyzer. To optimize the signal to noise ratio, 20,000 photon counts (10,000 photon counts for time-resolved fluorescence anisotropy measurements) were collected in the peak channel. All experiments were performed using excitation and emission slits with a nominal bandpass of 2 nm or less. The data stored in a multichannel analyzer was routinely transferred to an IBM PC for analysis. Fluorescence intensity decay curves so obtained were deconvoluted with the instrument response function and analyzed as a sum of exponential terms:

$$F(t) = \Sigma_i \alpha_i \exp(-t/\tau_i) \quad (2)$$

where $F(t)$ is the fluorescence intensity at time t and α_i is a preexponential factor representing the fractional contribution to the time-resolved decay of the component with a lifetime τ_i such that $\sum_i \alpha_i = 1$. The decay parameters were recovered using a nonlinear least squares iterative fitting procedure based on the Levenberg–Marquardt algorithm [38,39]. The homemade software for iterative deconvolution also includes statistical and plotting subroutine packages. The goodness of the fit of a given set of observed data and the chosen function was evaluated by the reduced χ^2 ratio, the weighted residuals [40], and the autocorrelation function of the weighted residuals [41]. A fit was considered acceptable when plots of the weighted residuals and the autocorrelation function showed random deviation about zero with a minimum χ^2 value not more than 1.2. The fluorescence decays were analyzed by the discrete exponential analysis as well as the maximum entropy method (MEM). Mean amplitude-averaged lifetimes (τ_m) for triexponential decays of fluorescence were calculated from the decay times and preexponential factors using the following equation [37]:

$$\tau_m = \alpha_1\tau_1 + \alpha_2\tau_2 + \alpha_3\tau_3 \quad (3)$$

2.2.8. Maximum Entropy Method (MEM) analysis of fluorescence intensity decay

The fluorescence decay data analysis by MEM is a less biased and more robust way of data analysis [42–44]. In MEM, the fluorescence intensity decay ($I(t)$) is analyzed to the model of continuous distribution of lifetimes.

$$I(t) = \int_0^\infty \alpha(\tau)\exp(-t/\tau)d\tau \quad (4)$$

Here, $\alpha(\tau)$ represents the amplitude corresponding to the lifetime τ in the intensity decay. In practice, the limits on the above integration are set based on the information regarding the system under study and the detection limit of the instrument. In our case, the lower and the upper limits of the integration was set as 10 ps and 10 ns, respectively. For practical purposes, the above equation can be written in terms of a discrete sum of exponentials as

$$I(t) = \sum_{i=1}^{N} \alpha_i \exp(-t/\tau_i) \quad (5)$$

where N represents the total number of exponentials. In our data analysis, N is taken as 100 exponentials equally spaced in the $log(\tau)$ space between the lower and upper limits. MEM initially starts with a flat distribution of amplitudes $\alpha(\tau)$, i.e., each lifetime has equal contribution in the beginning and arrives at the amplitude distribution which best describes the observed experimental fluorescence intensity decay. The optimization of the amplitude distribution $\alpha(\tau)$ is carried out in successive cycles by minimizing the χ^2 value (close to 1.0) and maximizing the entropy (S) [42]. The expression used for S is the Shannon–Jayne's entropy function, which is

$$S = -\sum p_i \log p_i \quad \text{where } p_i = \alpha_i / \sum \alpha_i \quad (6)$$

Successive iterations provide distribution that minimize χ^2 and maximize S. If the χ^2 criterion is satisfied by many distributions in a particular iteration, then the distribution with maximum entropy is selected. The analysis is terminated when χ^2 reaches the specified lower limit or when χ^2 and $\alpha(\tau)$ show no change in successive iterations. MEM analysis gives a lifetime distribution that is model independent.

2.2.9. Analysis of time-resolved fluorescence anisotropy

For the measurement of time-resolved fluorescence anisotropy, Glan–Thompson prism polarizers were used. The fluorescence intensity decays were collected with the emission polarizer kept at parallel ($I_{||}$) and perpendicular ($I_\perp$) orientations with respect to the excitation polarizer. These polarized components were then corrected for the grating factor (G-factor). The G-factor is defined as the ratio of the transmission efficiency of the grating for vertically polarized light

to horizontally polarized light. The G-factor of the TCSPC set-up was measured by the area matching method, using Nile Red in a homogeneous solvent such as methanol. Using the experimentally obtained G-factor, for the sample whose anisotropy decay was to be experimentally measured, $I_{\perp}$ was collected for the time $t_{||}G$ where $t_{||}$ is the time for which $I_{||}$ was collected. These two polarized intensity decays were used to compute the fluorescence anisotropy decay according to the following equation [37]:

$$r(t) = \frac{I_{||}(t) - I_{\perp}(t)}{I_{||}(t) + 2I_{\perp}(t)} \tag{7}$$

where

$$I_{||}(t) = I(t)[1 + 2r(t)]/3$$

and

$$I_{\perp}(t) = I(t)[1 - r(t)]/3$$

The equation for time resolved fluorescence anisotropy for any system can be expressed as

$$r(t) = (r_0 - r_{\infty}) \sum_{j=1}^{M} \beta_j \exp(-t/\phi_j) + r_{\infty} \tag{8}$$

where, ϕ_j and β_j represents the jth rotational correlation time and the corresponding pre-exponential factor in the M exponential anisotropy decay with $\sum\beta_i = 1$. r_0 and r_{∞} represent the anisotropies at zero time (initial anisotropy) and at infinite time (residual anisotropy) respectively. The goodness of the fit of a given set of observed data and the chosen function was evaluated by the reduced χ^2 ratio which ranged between 1.0 and 1.2. The initial anisotropy r_0 was determined to be 0.33 at excitation and emission wavelength of 575 and 620 nm, respectively (2.5 μM Nile Red in 100% glycerol; time per channel as 80 ps). The residual anisotropy r_{∞} in the anisotropy equation above represents the rotational freedom of the molecule. When the probe is in a homogeneous medium where it can rotate freely in all directions, r_{∞} becomes zero. However, this is not true if the probe is in a restricted environment in the time range when the anisotropy is measured.

In the case of membranes, the anisotropy gets depolarized not only because of the rotational motion of the probe but also due to the global or segmental motion of the membrane components. If ϕ_L denotes correlation time for the restricted local motion of the probe and ϕ_M the correlation time for the segmental motion of the membrane components, then the above equation can be written as follows [37]:

$$r(t) = \{(r_0 - r_{\infty})\exp(-t/\phi_L) + r_{\infty}\}\exp(-t/\phi_M) \tag{9}$$

which can be simplified as

$$r(t) = (r_0 - r_{\infty})\exp\left(-t\left(\frac{1}{\phi_L} + \frac{1}{\phi_M}\right)\right) + r_{\infty}\exp(-t/\phi_M) \tag{10}$$

Upon comparing the above two equations, we can show that

$$\phi_1 = \left(\frac{1}{\phi_L} + \frac{1}{\phi_M}\right)^{-1} \tag{11}$$

$$\phi_2 = \phi_M$$

It is interesting to note that when $\phi_L \lll \phi_M$, $\phi_1 \cong \phi_L$, and when $\phi_M \to \infty$, Eq. (10) becomes (8).

3. Results

3.1. Fluorescence characteristics of Nile Red in hippocampal membranes

Nile Red fluorescence is known to be sensitive to the polarity of the medium, i.e., the dielectric environment. In a polar environment, Nile Red has a low fluorescence quantum yield, whereas in more hydrophobic environments its quantum yield increases and its emission maximum becomes progressively blue shifted [26–28,45]. We have recently shown that the fluorescence emission maximum of Nile Red in dioleoyl-*sn*-glycero-3-phosphocholine (DOPC) membranes displays a shift toward lower wavelength (blue shift) in presence of cholesterol [45]. The intensity-normalized excitation and emission spectra of Nile Red in native membranes are shown in Fig. 1, and the fluorescence emission maximum was found to be 588 nm (see Table 1). We carried out cholesterol depletion in native hippocampal membranes using MβCD. MβCD is a water-soluble compound, and has previously been shown to selectively and efficiently extract cholesterol from hippocampal membranes by including it in a central nonpolar cavity [18]. Table 2 shows that upon treatment with increasing concentrations of MβCD, the cholesterol content of bovine hippocampal membranes decreases progressively resulting in a reduction in cholesterol/phospholipid ratio (mol/mol). This effect levels off with

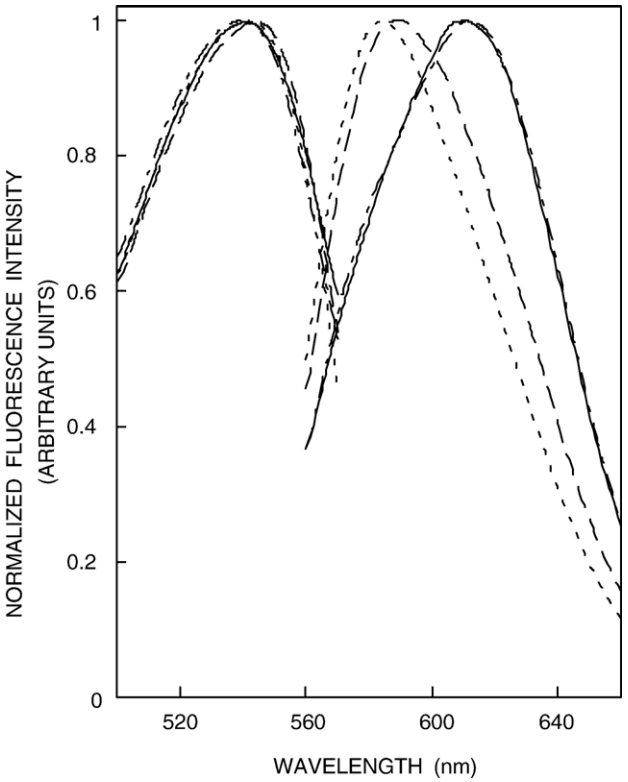

Fig. 1. Fluorescence excitation and emission spectra of Nile Red in native hippocampal membranes (– –), cholesterol-depleted (with 40 mM MβCD) membranes (—), liposomes of lipid extract from native membranes (- - -), and liposomes of lipid extract from cholesterol-depleted (with 40 mM MβCD) membranes (–·–). The spectra are intensity-normalized at the respective excitation and emission maximum. The emission wavelength was 582 nm for the excitation spectra and the excitation wavelength used was 545 nm for recording the emission spectra in all cases. The individual excitation and emission maxima are listed in Table 1. The protein concentration was ~0.04 mg/ml. Phospholipid concentration was 0.07 mM and the ratio of fluorophore (Nile Red) to total phospholipid was maintained at 1:50 (mol/mol). See Materials and methods for other details.

Table 1
Effect of cholesterol depletion on fluorescence excitation and emission maxima[a] of Nile Red in native membranes and lipid extracts[b]

Membrane condition	Excitation maximum (nm)[c]	Emission [d]
Native	542	588
Cholesterol-depleted membranes (with 40 mM MβCD)	541	610
Lipid extract from native membranes	541	584
Lipid extract from cholesterol-depleted membranes (depletion with 40 mM MβCD)	540	611

[a] We have used the term maximum of fluorescence emission in a somewhat wider sense here. In every case, we have monitored the wavelength corresponding to maximum fluorescence intensity, as well as the center of mass of the fluorescence emission. In most cases, both these methods yielded the same wavelength. In cases where minor discrepancies were found, the center of mass of emission has been reported as the fluorescence maximum.
[b] The ratio of Nile Red to total phospholipids is 1:50 (mol/mol). The concentration of Nile Red was 2 μM.
[c] Emission wavelength was 582 nm. See Materials and methods for other details.
[d] Excitation wavelength was 545 nm. See Materials and methods for other details.

increasing concentrations of MβCD (see Table 2). Importantly, we have previously shown that the change in phospholipid content under these conditions is negligible [18–20]. This shows that the depletion of cholesterol by MβCD is predominantly specific (see also [18]). The emission maximum of Nile Red in cholesterol-depleted hippocampal membranes (when treated with 40 mM MβCD) was found to be 610 nm (Fig. 1 and Table 1). The emission maximum therefore displays a red shift of 22 nm (from 588 to 610 nm) upon cholesterol depletion (see Fig. 1 and Table 1), in agreement with our previous results using model membranes [45]. This indicates that Nile Red experiences a more polar environment upon depletion of cholesterol. This is contrary to earlier results which indicated that cholesterol decreases hydrophobicity (increases water penetration) from the polar headgroup region to a depth of approximately carbon-9 of the phospholipid acyl chain [46], especially keeping in mind the interfacial localization of Nile Red in the membrane [45]. While this is somewhat surprising, it brings out the fact that the fluorescence emission maximum is influenced by a number of environmental factors and it is not always easy to interpret peak shifts in emission maximum, especially in microheterogeneous media such as membranes. On the other hand, the emission maximum of Nile Red in liposomes from lipid extract of native membranes is 584 nm (see Table 1), closer to that of native membranes. Interestingly, the emission maximum of Nile Red in lipid extracts made from cholesterol-depleted membranes (611 nm) is similar to that of cholesterol-depleted native membranes.

3.2. Lifetime distribution and fluorescence anisotropy of Nile Red in hippocampal membranes

Representative fluorescence intensity decay profiles of Nile Red incorporated in hippocampal membranes and cholesterol-depleted membranes with its triexponential fitting and various statistical parameters used to check the goodness of the fit are shown in Fig. 2. The resultant lifetime distributions obtained by MEM analysis are shown in Fig. 3. The peak positions and widths of the lifetime distribution (FWHM, full-width at half maximum) obtained from MEM analysis of fluorescence decay kinetics of Nile Red in native membranes as a function of cholesterol depletion (when treated with increasing concentrations of MβCD) are shown in Figs. 4b and 5. respectively.

Fluorescence lifetimes of Nile Red under various conditions were also analyzed by the discrete analysis method (see Table 3). We chose to use the mean fluorescence lifetime as an important parameter for describing the behavior of Nile Red incorporated into membranes since it is independent of the number of exponentials used to fit the time-resolved fluorescence decay. The mean fluorescence lifetimes of Nile Red in native and cholesterol-depleted membranes as well as in liposomes of lipid extracts from native membranes are shown in Table 3 (also see Fig. 4a). As seen from the table, all fluorescence decays could be fitted well with a triexponential function. The mean fluorescence lifetimes of Nile Red in these membranes were calculated using Eq. (3) and shown in the last column of Table 3. The lifetime of Nile Red in hippocampal membranes is found to be ~3.57 ns. This is consistent with earlier literature values since the lifetime of Nile Red incorporated in various membranes have previously been reported to be ~3–4 ns [25,45,47]. More importantly, the mean fluorescence lifetimes and the peak positions (from resultant lifetime distribution obtained by MEM analysis) of Nile Red in hippocampal membranes decrease with increasing concentrations of MβCD, i.e., as a function of cholesterol depletion (see Figs. 4a, b). The percentage change in mean fluorescence lifetime upon cholesterol depletion (when treated with 40 mM MβCD) is ~18%. In water, however, Nile Red lifetime reduces to ~1.6 ns [47], which could be attributed to hydrogen bonding interactions between the fluorophore and the solvent [45]. It is well known that fluorescence lifetime of Nile Red is sensitive to solvent properties, temperature, and excited-state interactions [26–28]. This is in agreement with our earlier results in which it was shown that the fluorescence lifetime of Nile Red increases with increase in cholesterol content of the membrane [45]. Interestingly, there is significant reduction in mean fluorescence lifetime of Nile Red upon

Table 2
Cholesterol/phospholipid ratio in hippocampal membranes with increasing cholesterol depletion

Membrane condition	Cholesterol/phospholipid (mol/mol)
Native	0.45
Native membranes treated with	
(i) 10 mM MβCD	0.34
(ii) 20 mM MβCD	0.19
(iii) 30 mM MβCD	0.13
(iv) 40 mM MβCD	0.07

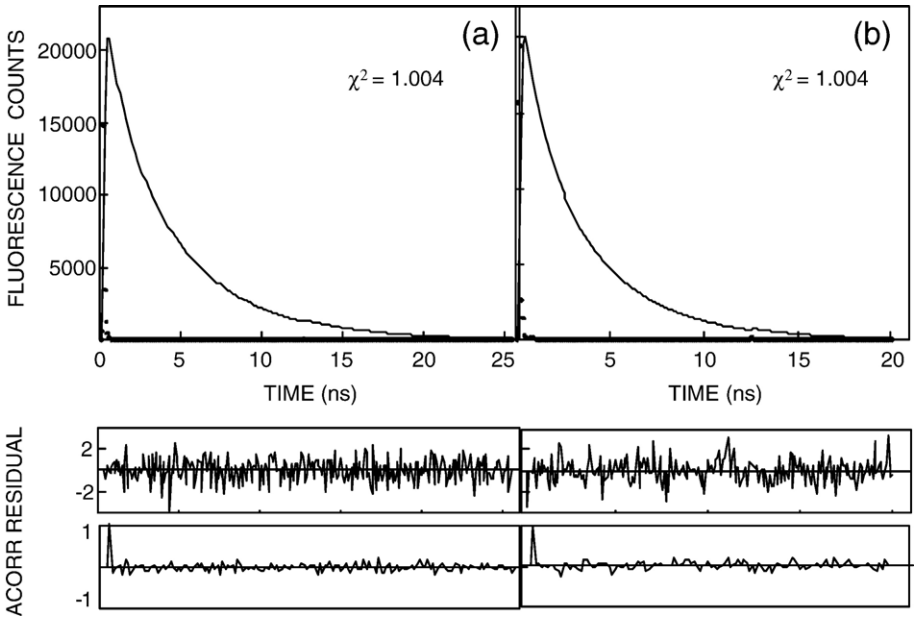

Fig. 2. Typical time-resolved fluorescence intensity decays of Nile Red in (a) native hippocampal membranes and (b) cholesterol-depleted (with 40 mM MβCD) membranes. The excitation wavelength was 575 nm and emission was monitored at 620 nm. The sharp peak on the left corresponds to the laser pulse. The decay profile on the right is fitted to a triexponential function. The two lower plots show the weighted residuals and the autocorrelation function of the weighted residuals. The protein concentration was ~0.04 mg/ml. Phospholipid concentration was 0.03 mM and the ratio of fluorophore (Nile Red) to total phospholipid was maintained at 1:100 (mol/mol). See Materials and methods for other details.

depletion of protein from the hippocampal membrane (see Table 3).

The steady state fluorescence anisotropy (r_{ss}) of Nile Red incorporated in hippocampal membranes as a function of increasing cholesterol depletion is shown in Fig. 4c. The fluorescence anisotropy (r_{ss}) of Nile Red shows a significant decrease with progressive depletion of cholesterol indicating an overall decrease in membrane order as monitored by Nile Red. In order to ensure that the observed change in anisotropy of Nile Red in native membranes (Fig. 4c) is not due to any change in lifetime (see Table 3 and Fig. 4a), the apparent rotational correlation times for Nile Red were calculated using Perrin's equation [37]:

$$\phi_{\text{apparent}} = \frac{\tau_m r_{ss}}{r_o - r_{ss}} \tag{12}$$

where r_o is the limiting anisotropy of Nile Red, and τ_m is the mean fluorescence lifetime as calculated from Eq. (3). The values of the apparent rotational correlation times, calculated this way using a value of r_o of 0.33 [25], are shown in Fig. 4d with increasing cholesterol depletion. The apparent rotational correlation time represents the overall rotational dynamics of Nile Red in these membranes. The progressive reduction in apparent rotational correlation time with increasing cholesterol depletion therefore indicates that the rotational dynamics becomes faster upon removal of cholesterol (Fig. 4d). Importantly, the overall trend in the change in apparent rotational correlation times with cholesterol depletion parallels the observed change in fluorescence anisotropy. This ensures that the observed change in anisotropy values is free from lifetime-induced artifacts.

3.3. Correlation of the width of the lifetime distribution with the cholesterol- and protein-induced heterogeneity in hippocampal membranes

Fluorescence decay kinetics of probes incorporated in complex systems generally display a considerable level of heterogeneity. The lifetime distribution of fluorescent probes represents a powerful method for characterizing complex systems such as membranes. The width of the lifetime distribution has been used to interpret the integrity and heterogeneity of membranes [24,25,48]. Nile Red lifetime distribution in the native membrane was found to be significantly broader as compared to that of the cholesterol-depleted membrane (see Figs. 3 and 5). This is consistent with the previous observation that cholesterol increases the width of the lifetime distribution of Nile Red incorporated in model [25,48] and cell [24] membranes. The peak position (Fig. 4b) and the width of the lifetime distribution (Fig. 5) shows a progressive reduction with increasing cholesterol depletion from native hippocampal membranes. This clearly shows that the extent of heterogeneity decreases with decrease in membrane cholesterol content. Interestingly, Nile Red lifetime distribution in liposomes of lipid extracts is similar to that of native membranes indicating that proteins do not contribute significantly to the high level of heterogeneity observed in native membranes (see Figs. 3b and 7c).

The observed decrease in the width of the lifetime distribution (FWHM) with depletion of cholesterol from native membranes (see Fig. 5) is interesting. We confirmed that the increase in the width of the lifetime distribution was real and not an artifact caused by factors such as an inadequate signal to

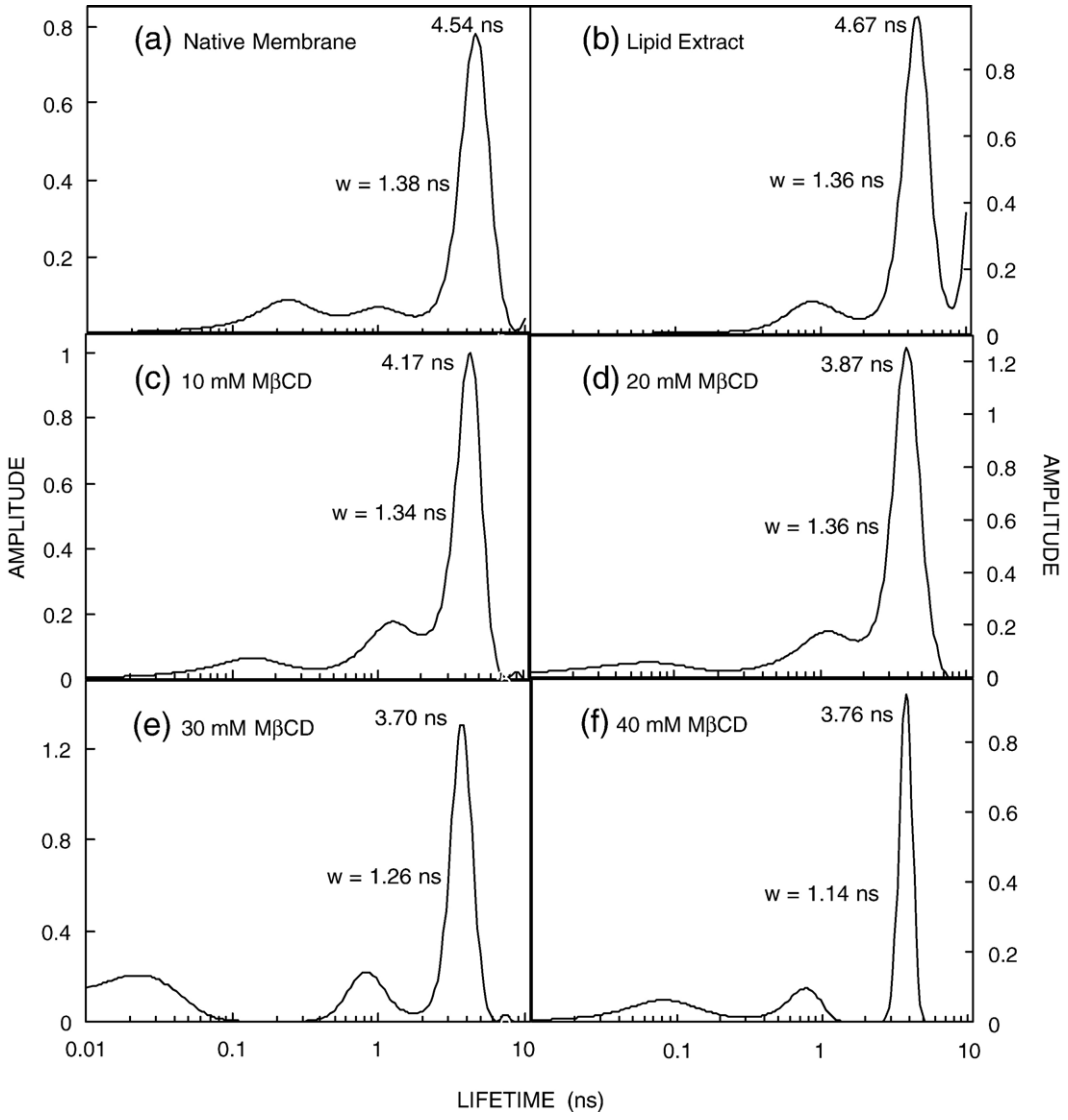

Fig. 3. MEM lifetime distribution of Nile Red in (a) native hippocampal membranes and in native membranes treated with (c) 10, (d) 20, (e) 30, and (f) 40 mM MβCD, and in (b) liposomes of lipid extract from native membranes. Here 'w' represents the width of the fluorescence lifetime distribution (represented as full width at half maximum, FWHM) for the major peak whose positions are indicated on the respective distributions. All other conditions are as in Fig. 2. See Materials and methods for other details.

noise ratio, and collection of incomplete decay [44]. This was achieved by monitoring the width of the lifetime distribution as a function of the signal to noise ratio of the collected data (represented by the count in the peak channel). The limiting width obtained at a high signal to noise ratio was taken as the real width demanded by the system [24,25,44,48].

We found an increase in the width of the lifetime distribution with increasing cholesterol content clearly indicating cholesterol-induced heterogeneity in bovine hippocampal membranes (Figs. 3 and 5). Cholesterol is often found distributed non-randomly in domains or pools in biological and model membranes [11–15] and many of these domains are believed to be important for the maintenance of membrane structure and function [7,12,22,49]. However, detailed spatiotemporal characterization of such domains is only beginning to be addressed [49]. The broad distribution of lifetimes obtained here shows that the structure of cholesterol-induced domains is highly heterogeneous. These results are in agreement with our previous observation that the cooperativity index of the apparent thermal phase transition, as monitored by changes in Laurdan excitation generalized polarization (excitation GP), shows an increase upon cholesterol depletion [19]. This indicates that cholesterol depletion results in a relatively homogeneous membrane.

3.4. Time-resolved anisotropy of Nile Red in hippocampal membranes

The information about the rotational dynamics is provided by the time-resolved anisotropy of Nile Red. Fig. 6a shows the time-resolved decay of fluorescence anisotropy of Nile Red in native hippocampal membranes and cholesterol-depleted membranes. The kinetics could be fitted to a sum of three exponentials, and the values of the rotational correlation time (ϕ) are given in Table 4. The time-resolved anisotropy of Nile

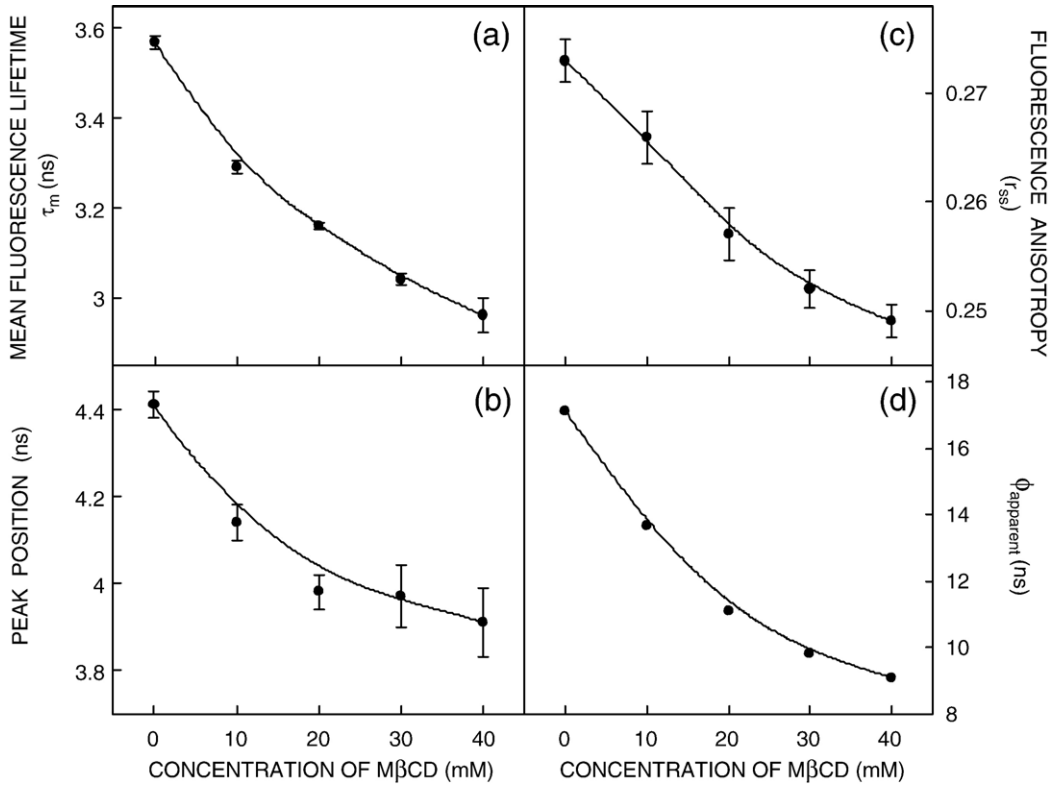

Fig. 4. Effect of cholesterol depletion on (a) mean fluorescence lifetime (τ_m), (b) peak value of the fluorescence lifetime (calculated from MEM distribution of Nile red), (c) steady state fluorescence anisotropy (r_{ss}), and (d) apparent rotational correlation time ($\phi_{apparent}$) of Nile Red in native hippocampal membranes. Mean fluorescence lifetimes were calculated from Table 3 using Eq. (3). All other conditions are as in Fig. 2, except for steady state fluorescence anisotropy (panel c) for which conditions are as in Fig. 1. The excitation wavelength used was 545 nm and emission was monitored at 585 nm for steady-state fluorescence anisotropy measurements. The apparent rotational correlation times were calculated using Eq. (12). The data points shown are the means ± S.E. of at least three independent measurements. See Materials and methods for other details.

Red in membranes showed at least three rotational correlation times (see Table 4): ϕ_1 in the range of 0.2–0.4 ns (local motion), ϕ_2 in the range of 12–16 ns (segmental motion) and ϕ_3 is longer than 200 ns (global motion). The lower limit of ϕ_3 comes from our observation window of ~35 ns, which is dictated by the fluorescence lifetime. However, ϕ_2, which represents the segmental motion of Nile Red (relevant in the context of membrane lipid dynamics) within a cone defined by the relative amplitudes [50], show a relatively weak dependence on the depletion of cholesterol from the native membrane (see Fig. 6b). Fig. 6b shows that ϕ_2 (which represents the overall trend of rotational correlation time amongst the three rotational correla-

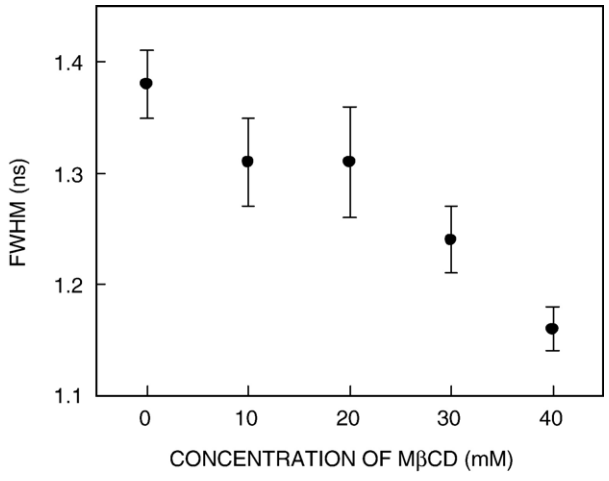

Fig. 5. Effect of cholesterol depletion on the width of the Nile Red lifetime distribution (FWHM) for the major peak in native hippocampal membranes. FWHM values were calculated from MEM distribution of Nile red. All other conditions are as in Fig. 2. The data points shown are the means ± S.E. of at least nine independent measurements. See Materials and methods for other details.

Table 3
Fluorescence lifetimes of Nile Red in native and cholesterol-depleted membranes and in lipid extract [a]

Membrane condition	α_1	τ_1 (ns)	α_2	τ_2 (ns)	α_3	τ_3 (ns)	τ_m [b] (ns)
Native	0.23	5.63	0.58	3.65	0.19	0.85	3.57
Native membranes treated with							
(i) 10 mM MβCD	0.45	4.87	0.37	2.66	0.18	0.69	3.29
(ii) 20 mM MβCD	0.54	4.45	0.32	2.12	0.14	0.50	3.15
(iii) 30 mM MβCD	0.53	4.17	0.30	2.27	0.17	0.63	3.00
(iv) 40 mM MβCD	0.50	4.32	0.35	2.21	0.15	0.52	2.94
Lipid extract	0.17	5.50	0.58	2.57	0.25	0.50	2.55

[a] Excitation wavelength was 575 nm and emission was monitored at 620 nm. All other conditions are as in Fig. 4a and 7a. The errors were ~10% for all the parameters except τ_m for which the error was ~5%. See Materials and methods for other details.

[b] Calculated using Eq. (3).

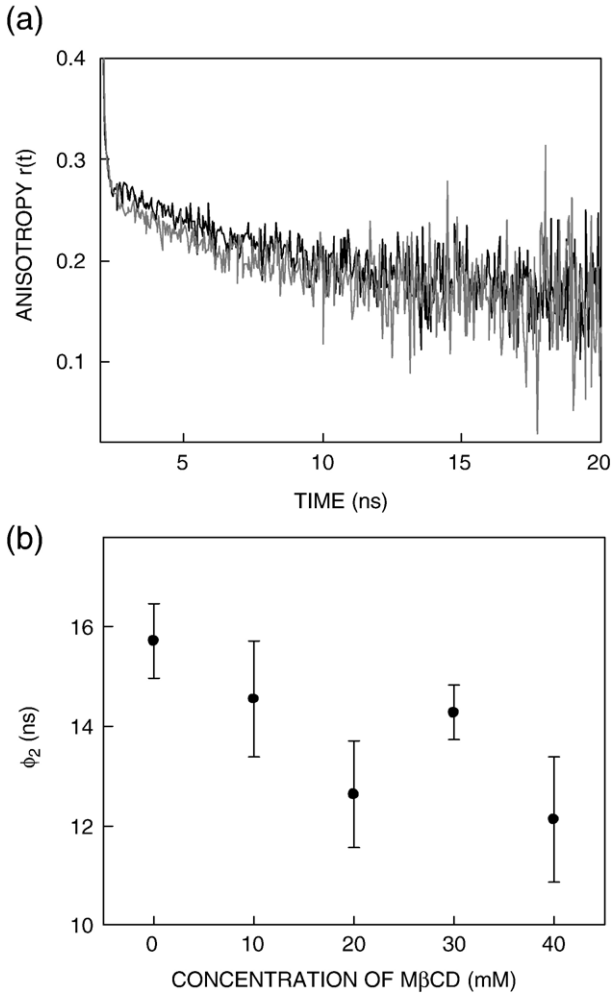

Fig. 6. (a) Time-resolved fluorescence anisotropy decay of Nile Red in native hippocampal membranes (black line) and cholesterol-depleted (with 40 mM MβCD) membranes (gray line) at 23 °C, and (b) effect of cholesterol depletion on the second component of rotational correlation time (ϕ_2) of Nile Red in native membranes. All other conditions are as in Fig. 2. The data points shown are the means±S.E. of at least nine independent measurements. See Materials and methods for other details.

tion times, as $\phi_2 \approx \phi_{\text{apparent}}$) shows a decrease (~25%) as a function of cholesterol depletion in native hippocampal membranes (also see Table 4).

3.5. Temperature dependence of lifetime distribution, the width of the lifetime distribution and fluorescence anisotropy of Nile Red in hippocampal membranes

The mean fluorescence lifetimes of Nile Red in native membranes and liposomes of lipid extracts from native membranes as a function of increasing temperature (0–60 °C) are shown in Table 5 (also see Fig. 7a). As seen from the table, all fluorescence decays could be fitted well with a triexponential function. The mean fluorescence lifetimes of Nile Red in these membranes were calculated using Eq. (3) and shown in the last column of Table 5. The lifetime of Nile Red in hippocampal membranes as a function of increasing temperature decreases from ~3.8 to 1.7 ns (~55%). Interestingly, this is well

Table 4
Time-resolved fluorescence anisotropy decay of Nile Red in native and cholesterol-depleted membranes [a]

Membrane condition	β_1	ϕ_1 (ns)	β_2	ϕ_2 (ns)	β_3	ϕ_3 (ns)	r_0 [b]
Native	0.23	0.13	0.43	15.72	0.34	>200	0.330
Native membranes treated with							
(i) 10 mM MβCD	0.22	0.21	0.44	14.54	0.34	>200	0.333
(ii) 20 mM MβCD	0.22	0.35	0.44	12.62	0.34	>200	0.329
(iii) 30 mM MβCD	0.20	0.38	0.46	14.27	0.34	>200	0.330
(iv) 40 mM MβCD	0.27	0.19	0.39	12.12	0.34	>200	0.330

[a] Excitation wavelength was 575 nm and emission was monitored at 620 nm. The errors were ~15% for ϕ_1 and ~10% for other parameters. All other conditions are as in Fig. 6. See Materials and methods for other details.
[b] r_0 is the initial anisotropy of Nile Red, and was determined in an independent experiment with excitation and emission wavelength of 575 and 620 nm respectively (2.5 μM Nile Red in 100% glycerol; time per channel as 80 ps). The value of r_0 was kept constant at 0.33 in the analysis.

supported by a corresponding decrease in the peak value of the fluorescence lifetime (Fig. 7b) of Nile Red obtained using the MEM approach in native membranes as a function of increasing temperature. The reduction of fluorescence lifetime appears to indicate an increase in effective polarity in the membrane with increase in temperature, which could be attributed to water penetration in the membrane [19,25]. Alternatively, this could be the result of enhanced non-radiative decay with increase in temperature. In addition, there is a significant decrease in mean fluorescence lifetime and the peak position (from MEM analysis) of Nile Red in liposomes of lipid extracts from native membranes (see Figs. 7a and b) as a function of increasing temperature.

The widths of the lifetime distribution (FWHM) by MEM analysis of native membranes and liposomes of lipid extracts from native membranes as a function of increasing temperature (0–60 °C) are shown in Fig. 7c. The width of the lifetime distribution shows a decrease with increasing temperature in the region 0–20 °C and nearly constant thereafter. In general, decrease in the width of lifetime distribution with increase in temperature could be due to an increase in the translational dynamics of the probe resulting in more efficient averaging of

Table 5
Fluorescence lifetimes of Nile Red in native membranes with increasing temperature [a]

Temperature (°C)	α_1	τ_1 (ns)	α_2	τ_2 (ns)	α_3	τ_3 (ns)	τ_m [b]
0	0.54	5.69	0.27	2.31	0.19	0.66	3.82
5	0.33	6.25	0.40	3.61	0.27	0.76	3.71
15	0.48	5.83	0.28	2.34	0.24	0.60	3.60
25	0.23	5.63	0.58	3.65	0.19	0.85	3.57
35	0.43	4.66	0.24	2.08	0.33	0.54	2.68
45	0.48	3.89	0.19	1.41	0.33	0.46	2.29
55	0.21	4.04	0.31	2.59	0.48	0.47	1.88
60	0.17	3.92	0.33	2.38	0.50	0.41	1.66

[a] Excitation wavelength was 575 nm and emission was monitored at 620 nm. All other conditions are as in Fig. 7a. The errors were ~10% for all the parameters except τ_m for which the error was ~5%. See Materials and methods for other details.
[b] Calculated using Eq. (3).

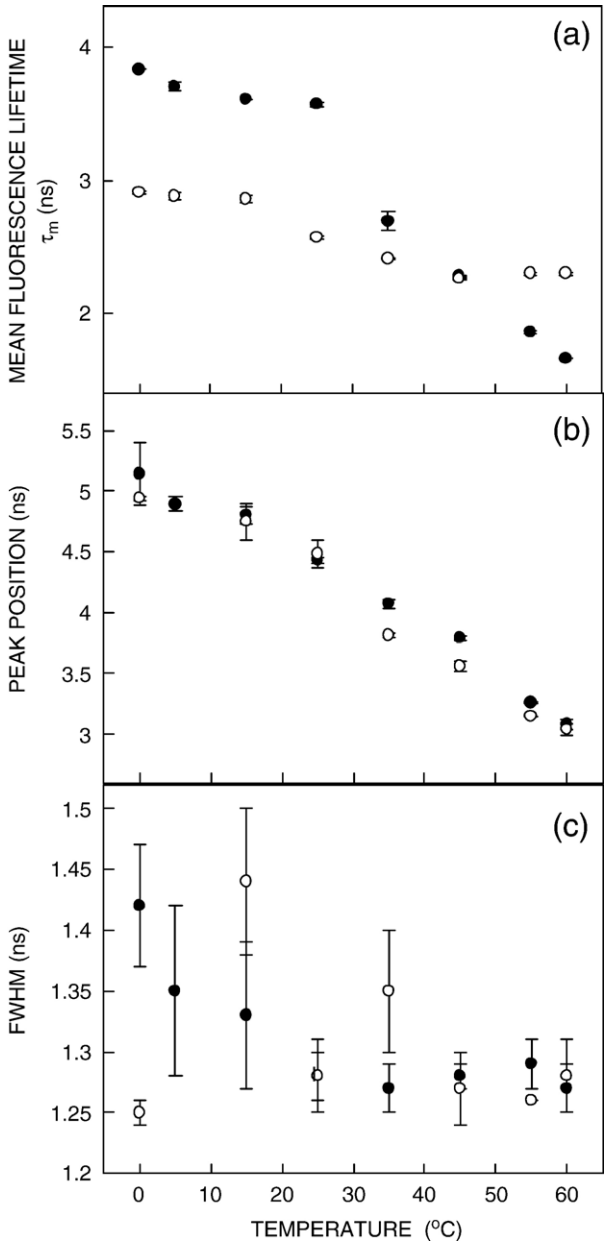

Fig. 7. Temperature dependence of (a) mean fluorescence lifetime (τ_m), (b) peak value of the fluorescence lifetime (calculated from MEM distribution of Nile red), and (c) the width of the Nile Red lifetime distribution (FWHM) in native hippocampal membranes (●) and in liposomes of lipid extract from native membranes (○). Mean fluorescence lifetimes were calculated from Table 5 using Eq. (3). FWHM values were calculated from MEM distribution of Nile red. All other conditions are as in Fig. 2. The data points shown are the means±S.E. of at least nine independent measurements. See Materials and methods for other details.

its environment during the lifetime of the probe. However, the trend in FWHM with temperature appears noisy and the decrease in FWHM does not appear to be substantial keeping in mind the temperature range (0–60 °C). FWHM of lifetime distribution could decrease only if the probe samples all the environments during its excited state lifetime. However, this may not be possible given the diffusion coefficient of the probe in its excited state lifetime. Any realistic increase in the translational dynamics in this temperature range therefore is unlikely to result in effective averaging of environment around the probe (see later). Another probable reason for no substantial change in heterogeneity from 20 to 60 °C could be the limiting width of Nile Red which is limited by the available signal to noise ratio. However, this is unlikely since the width observed in DMPC membranes is in the range of 0.4–0.6 ns [24,25]. Nile Red lifetime distribution in liposomes of lipid extracts from native membranes is similar to that of the native membrane at higher temperatures (>20 °C) (see Fig. 7c). Interestingly, the level of heterogeneity appears to be more or less constant in the temperature range of 20–60 °C. Therefore, it appears that the extent of heterogeneity characteristic of the native hippocampal membrane (at ~20 °C) does not reduce significantly at high temperature (up to 60 °C) and the native heterogeneity is preserved even at high temperatures.

The steady state fluorescence anisotropy (r_{ss}) of Nile Red incorporated in native membranes and cholesterol-depleted membranes with increasing temperature is shown in Fig. 8a. The fluorescence anisotropy (r_{ss}) of Nile Red shows a significant decrease with increasing temperature both in native

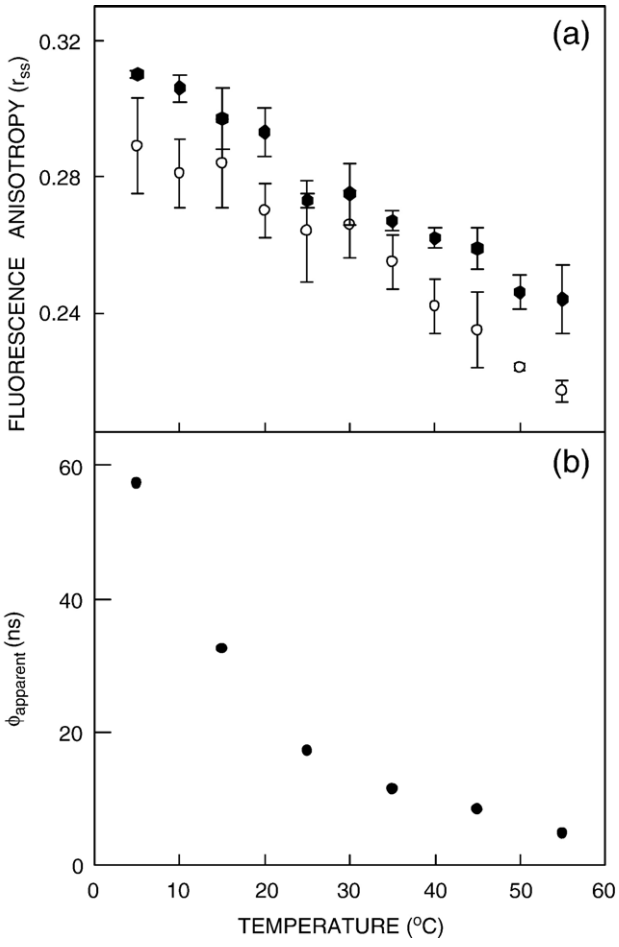

Fig. 8. (a) Temperature dependence of steady state fluorescence anisotropy (r_{ss}) of Nile Red in native hippocampal membranes (●) and cholesterol-depleted (with 40 mM MβCD) membranes (○). (b) Temperature dependence of apparent rotational correlation time ($\phi_{apparent}$) of Nile Red in native hippocampal membranes. All other conditions are as in Fig. 4. The data points shown are the means±S.E. of at least three independent measurements. See Materials and methods for other details.

and cholesterol-depleted membranes, indicating a reduction in membrane order. In order to ensure that the observed change in anisotropy of Nile Red in native membranes (Fig. 8a) is not due to any change in lifetime (see Table 5 and Fig. 7a), the apparent rotational correlation times for Nile Red were calculated using Perrin's equation (Eq. (12)). The values of the apparent rotational correlation times, calculated this way using a value of r_o of 0.33 [25], are shown in Fig. 8b. The overall trend in the change in apparent rotational correlation times with increasing temperature parallels the observed change in anisotropy. This ensures that the observed change in anisotropy values is free from lifetime-induced artifacts.

3.6. Temperature dependence of time-resolved anisotropy of Nile Red in hippocampal membranes

Fig. 9a shows the time-resolved decay of fluorescence anisotropy of Nile Red in native hippocampal membranes as a function of temperature. As described earlier, the kinetics could be fitted to a sum of three exponentials, and the values of the rotational correlation time (ϕ) are given in Table 6: ϕ_1 in the range of 0.1–0.12 ns (local motion), ϕ_2 in the range of 3–54 ns (segmental motion) and ϕ_3 is longer than 200 ns (global motion). Since $\phi_{apparent} \geq \tau_m$ (where τ_m is the fluorescence lifetime of Nile Red), the rotational motion is not expected to effectively average the environment around Nile Red. The lower limit of ϕ_3 comes from our observation window of ~35 ns, which is dictated by the fluorescence lifetime. However, ϕ_2, which represents the segmental motion of Nile Red (relevant in the context of lipid dynamics in the membrane) within a cone defined by the relative amplitudes [50], shows a strong dependence with temperature (see Fig. 9b). Fig. 9b shows that ϕ_2 (which represents the overall trend of rotational correlation time amongst the three rotational correlation times, as $\phi_2 \approx \phi_{apparent}$) shows a substantial reduction (~95%) as a function of increasing temperature in native hippocampal membranes (also see Table 6). This further supports our earlier observation where a decrease in membrane order has been indicated with increased temperature in native hippocampal membranes [19].

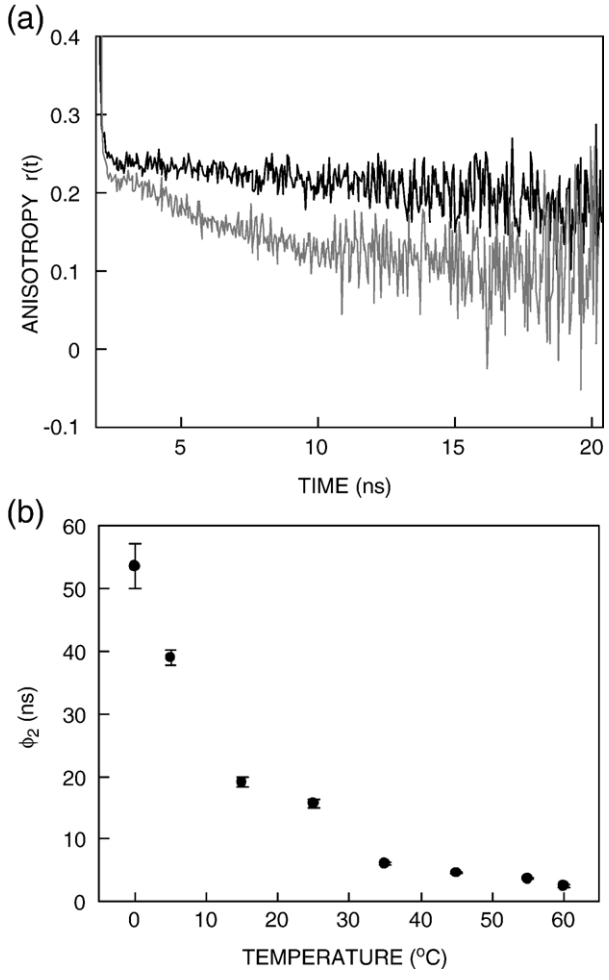

Fig. 9. (a) Time-resolved fluorescence anisotropy decay of Nile Red in native hippocampal membranes at 0 (black line) and 45 °C (gray line), and (b) change in the second component of rotational correlation time (ϕ_2) of the Nile Red in native membranes as a function of increasing temperature. All other conditions are as in Fig. 2. The data points shown are the means±S.E. of at least nine independent measurements. See Materials and methods for other details.

Table 6
Time-resolved fluorescence anisotropy decay of Nile Red in native membranes with increasing temperature[a]

Temperature (°C)	β_1	ϕ_1 (ns)	β_2	ϕ_2 (ns)	β_3	ϕ_3 (ns)	r_0[b]
0	0.22	0.12	0.44	53.52	0.34	>200	0.332
5	0.21	0.14	0.45	38.97	0.34	>200	0.331
15	0.20	0.10	0.46	19.09	0.34	>200	0.329
25	0.23	0.13	0.43	15.72	0.34	>200	0.330
35	0.27	0.10	0.42	6.11	0.31	>200	0.326
45	0.25	0.13	0.43	4.64	0.32	>200	0.329
55	0.25	0.10	0.42	3.73	0.33	>200	0.328
60	0.19	0.10	0.44	2.60	0.37	>200	0.330

[a] Excitation wavelength was 575 nm and emission was monitored at 620 nm. The errors were ~15% for $\phi_1$and ~10% for other parameters. All other conditions are as in Fig. 9. See Materials and methods for other details.
[b] r_0 is the initial anisotropy of Nile Red, and was determined in an independent experiment with excitation and emission wavelength of 575 and 620 nm respectively (2.5 μM Nile Red in 100% glycerol; time per channel as 80 ps). The value of r_0 was kept constant at 0.33 in the analysis.

4. Discussion

Although the membrane lipid composition of bovine hippocampus is not known, the phospholipid composition of rat hippocampus has recently been reported [51–53]. Analysis of the phospholipid composition of the rat hippocampus shows phosphatidylethanolamine, phosphatidylcholine, and phosphatidylserine as the predominant headgroups, while the fatty acid composition shows enrichment with 16:0, 18:0, 18:1, 18:2, 20:4, and 22:6 fatty acids. In addition, plasmalogens have been reported in rat hippocampus. In this paper, we have monitored the influence of cholesterol and proteins on the dynamics and heterogeneity of hippocampal membranes using fluorescence lifetime distribution analysis of Nile Red using the MEM approach and time-resolved fluorescence anisotropy measurements. Nile Red has been previously used as a fluorescent probe for monitoring hydrophobic surfaces in proteins [54], protein–

detergent complexes [55], and as a lipid stain in membranes [56,57]. Knowledge of membrane dynamics would help in analyzing functional data generated by modulation of membrane lipid composition [4,18]. The interaction between cholesterol and other molecular components in neuronal membranes (such as receptors and lipids) assumes relevance for understanding brain function. The organization and dynamics of cellular membranes in the nervous system is therefore significant for a comprehensive understanding of the functional roles played by the membrane-bound neuronal receptors which are key components in signal transduction in the nervous system. Fluorescence lifetime distribution analysis of membrane probes represents a powerful and sensitive tool in characterizing the membrane organization and dynamics through the heterogeneity of population of the probe [24,25,48]. Nile Red has been used for monitoring organization, fluctuation, and heterogeneity in membranes, specifically for membranes containing cholesterol [24,25,45,56]. Unfortunately, the partitioning property of Nile Red in co-existing ordered and disordered phases is not known, and this would somehow limit detailed analysis of membrane heterogeneity. Importantly, analysis of membrane penetration depth using the parallax method points to an interfacial localization of Nile Red in membranes although it is predominantly a hydrophobic molecule [45].

4.1. Effect of cholesterol and proteins on the heterogeneity in hippocampal membranes

Our results show that the emission maximum of Nile Red in cholesterol-depleted hippocampal membranes displays a red shift upon cholesterol depletion (Fig. 1 and Table 1), which indicates that Nile Red experiences a more polar environment upon depletion of cholesterol. This is in agreement with earlier literature in which it was shown using the polarity-sensitive probe Laurdan that cholesterol reduces the polarity of phospholipid bilayers [58]. The peak position (Fig. 4b) and the width of the lifetime distribution (Fig. 5) show a progressive reduction with increasing cholesterol depletion from native hippocampal membranes. The change in FWHM clearly shows that the extent of heterogeneity decreases with decrease in membrane cholesterol content. This is accompanied by a concomitant decrease of the fluorescence anisotropy and rotational correlation time of Nile Red in native hippocampal membranes with removal of cholesterol (see Figs. 4c, d, and 6). This is in agreement with our earlier observation in native hippocampal membranes where a decrease in membrane order [18,19] has been indicated with depletion of cholesterol. We could attribute the change in heterogeneity to the probable variation in the composition of near neighbors and environment around the Nile Red as a function of cholesterol depletion. Alternately, the observed change in heterogeneity could be correlated to the heterogeneity in hydrogen bonding of Nile Red with the surrounding water molecules [45].

The increase in the width of lifetime distribution caused by cholesterol in hippocampal membranes could be rationalized as due to (i) the presence of heterogeneous domains and (ii) the sampling rate (k) of these domains by Nile Red, which is slower than $\sim 3\times10^{8}$ s^{-1} (inverse of the fluorescence lifetime of Nile Red). The sampling rate could be inferred from the rotational and translational dynamics of Nile Red in the membrane. The translational diffusion coefficient (D) of small neutral molecules (such as Nile Red) in membranes is $\sim 10^{-8}$ to 10^{-9} cm^2/s [59]. One of us recently reported the translational (lateral) diffusion coefficient of lipophilic probes in bovine hippocampal membranes to be $\sim 10^{-9}$ cm^2/s [60]. Therefore, the average distance ($<x>=(4D_{trans}\ t)^{1/2}$ [59] traversed by Nile Red during the fluorescence lifetime in hippocampal membranes is $\sim$0.36 Å assuming t as 3.57 ns (fluorescence lifetime of Nile Red, see Table 3). Movement by this distance is unlikely to be sufficient for averaging the environment around the probe.

Proteins are essential components of biological membranes and an understanding of the interaction of membrane proteins with the bilayer lipid matrix is essential for the organization and function of membranes [61]. In order to examine whether proteins influence the observed change in dynamics and heterogeneity, we made measurements in liposomes of lipid extracts from native membranes which are devoid of protein but whose lipid composition reflects that of native membranes. Our results indicate that the emission maximum of Nile Red in liposomes from lipid extract of native membranes is closer to that of native membranes while that of liposomes from lipid extracts made from cholesterol-depleted membranes is similar to that of cholesterol-depleted membranes (Table 1). These observations point out that the microenvironment experienced by Nile Red is relatively insensitive to the presence of proteins in hippocampal membranes. Interestingly, Nile Red lifetime distribution in liposomes of lipid extracts is similar to that of native membranes indicating that proteins do not contribute significantly to the high level of heterogeneity observed in native membranes (Figs. 3b and 7c). This provides support for lipid vesicles as good biological membrane models.

4.2. Temperature dependence of heterogeneity in hippocampal membranes

Our results show a decrease in the mean fluorescence lifetime and the peak value of the fluorescence lifetime of Nile Red in hippocampal membranes as a function of increasing temperature (Figs. 7a, b). Although decrease in lifetime with increase in temperature could be due to a variety of non-radiative processes, this could possibly indicate an increase in effective polarity in the membrane with temperature because of water penetration in the membrane [19,25], in agreement with earlier literature in which the polarity-dependent probe Laurdan was used [62]. Interestingly, the width of the lifetime distribution (Fig. 7c) decreases with increase in temperature in the range of 0–20 °C suggesting some structural changes in the membrane architecture. Nile Red lifetime distribution in liposomes of lipid extracts from native membranes is similar to that of the native membrane at higher temperatures thereby indicating that proteins do not contribute significantly to the observed heterogeneity (Fig. 7c). Moreover, the extent of heterogeneity of the native hippocampal membrane appears to

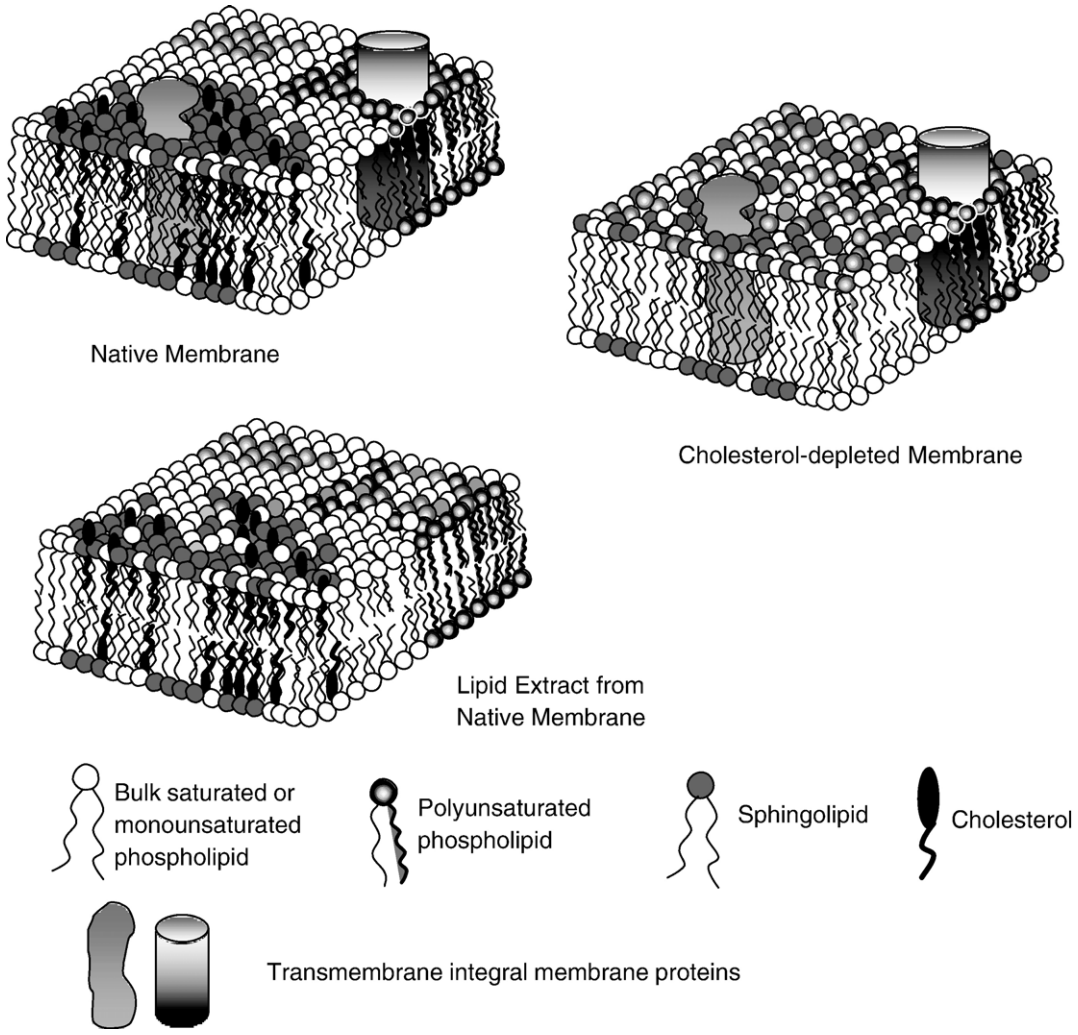

Fig. 10. A schematic representation of cholesterol-induced membrane heterogeneity in native hippocampal membranes. The native membrane is heterogeneous due to cholesterol-induced transient defects (as shown by the preferential association of lipids and proteins). Cholesterol-depletion results in reducing heterogeneity while proteins do not contribute significantly to the high level of heterogeneity observed in native membranes. See text for other details.

be preserved even at high temperatures. In addition, there is a substantial reduction in the rotational correlation times as a function of increasing temperature in hippocampal membranes. Again, a relatively large change in the rotational dynamics was observed in the temperature range 0–20 °C (Figs. 8b and 9b) supporting the model of structural changes in the membrane in this temperature range. Interestingly, we have previously reported that the overall membrane order of hippocampal membranes, as monitored by fluorescence polarization of 1,6-diphenyl-1,3,5-hexatriene (DPH), is maintained even at high temperatures [19]. A schematic representation of cholesterol- and protein-induced modulation of membrane heterogeneity in bovine hippocampal membranes is shown in Fig. 10.

Taken together, our results constitute one of the first reports on the dynamic heterogeneity in hippocampal membranes and its modulation by temperature, and membrane cholesterol and protein contents using fluorescence lifetime distribution and time-resolved anisotropy of Nile Red. This heterogeneity could arise from the cholesterol-induced transient structural defects in the membranes. Further, transient defects could increase the dynamic heterogeneity of the membrane, resulting in a broader distribution of the fluorescence lifetime of Nile Red. These results could be relevant in understanding the complex spatiotemporal organization of neuronal membranes, and may have functional implications in neuronal diseases such as the Smith–Lemli–Opitz syndrome [10,63] which is characterized by defective membrane sterol metabolism. In this syndrome, there is a reduction in tissue cholesterol levels due to defective biosynthesis of cholesterol which in turn leads to defective membrane organization, dynamics and function [64].

Acknowledgements

This work was supported by the Council of Scientific and Industrial Research (A.C.), and Department of Atomic Energy (G.K.), Government of India. S.M. thanks the Council of Scientific and Industrial Research for the award of a Senior Research Fellowship. A.C. is an Honorary Professor of the Jawaharlal Nehru Centre for Advanced Scientific Research, Bangalore (India). We gratefully acknowledge Md. Jafurulla

and Sandeep Shrivastava for help with the preparation of native membranes and cholesterol depletion from native membranes. Special thanks are due to T. Ramreddy, Anoop Saxena and Samrat Mukhopadhyay for helpful discussions. We thank Prof. N. Periasamy for providing the software for the analysis of MEM and time-resolved anisotropy data, and help with the analysis of fluorescence decay kinetics. We thank S. Rajanna, Shanti Kalipatnapu, Thomas Pucadyil, Md. Jafurulla, Sandeep Shrivastava, and Yamuna Devi Paila for help with the tissue collection and members of A.C.'s research group for critically reading the manuscript.

References

[1] M.R. Wenk, The emerging field of lipidomics, Nat. Rev., Drug Discov. 4 (2005) 594–610.
[2] P.S. Sastry, Lipids of nervous tissue: composition and metabolism, Prog. Lipid Res. 24 (1985) 69–176.
[3] K. Burger, G. Gimpl, F. Fahrenholz, Regulation of receptor function by cholesterol, Cell. Mol. Life Sci. 57 (2000) 1577–1592.
[4] T.J. Pucadyil, A. Chattopadhyay, Role of cholesterol in the function and organization of G-protein coupled receptors, Prog. Lipid Res. 45 (2006) 295–333.
[5] G.I. Papakostas, D. Öngür, D.V. Iosifescu, D. Mischoulon, M. Fava, Cholesterol in mood and anxiety disorders: review of the literature and new hypotheses, Eur. Neuropsychopharmacol. 14 (2004) 135–142.
[6] A. Chattopadhyay, Y.D. Paila, Lipid–protein interactions, regulation and dysfunction of brain cholesterol, Biochem. Biophys. Res. Commun. 354 (2007) 627–633.
[7] W.G. Wood, F. Schroeder, N.A. Avdulov, S.V. Chochina, U. Igbavboa, Recent advances in brain cholesterol dynamics: transport, domains, and Alzheimer's disease, Lipids 34 (1999) 225–234.
[8] J.J. Kabara, A critical review of brain cholesterol metabolism, Prog. Brain Res. 40 (1973) 363–382.
[9] S.D. Turley, D.K. Bruns, J.M. Dietschy, Preferential utilization of newly synthesized cholesterol for brain growth in neonatal lambs, Am. J. Physiol. 274 (1998) E1099–E1105.
[10] F.D. Porter, Malformation syndromes due to inborn errors of cholesterol synthesis, J. Clin. Invest. 110 (2002) 715–724.
[11] R.F.M. de Almeida, A. Fedorov, M. Prieto, Sphingomyelin/phosphatidylcholine/cholesterol phase diagram: boundaries and composition of lipid rafts, Biophys. J. 85 (2003) 2406–2416.
[12] K. Simons, E. Ikonen, Functional rafts in cell membranes, Nature 387 (1997) 569–572.
[13] X. Xu, E. London, The effect of sterol structure on membrane lipid domains reveals how cholesterol can induce lipid domain formation, Biochemistry 39 (2000) 843–849.
[14] K. Simons, E. Ikonen, How cells handle cholesterol, Science 290 (2000) 1721–1725.
[15] R. Rukmini, S.S. Rawat, S.C. Biswas, A. Chattopadhyay, Cholesterol organization in membranes at low concentrations: effects of curvature stress and membrane thickness, Biophys. J. 81 (2001) 2122–2134.
[16] T.J. Pucadyil, S. Kalipatnapu, A. Chattopadhyay, The serotonin1A receptor: a representative member of the serotonin receptor family, Cell. Mol. Neurobiol. 25 (2005) 553–580.
[17] A. Chattopadhyay, K.G. Harikumar, S. Kalipatnapu, Solubilization of high affinity G-protein-coupled serotonin1A receptors from bovine hippocampus using pre-micellar CHAPS at low concentration, Mol. Membr. Biol. 19 (2002) 211–220.
[18] T.J. Pucadyil, A. Chattopadhyay, Cholesterol modulates ligand binding and G-protein coupling to serotonin1A receptors from bovine hippocampus, Biochim. Biophys. Acta 1663 (2004) 188–200.
[19] S. Mukherjee, A. Chattopadhyay, Monitoring the organization and dynamics of bovine hippocampal membranes utilizing laurdan generalized polarization, Biochim. Biophys. Acta 1714 (2005) 43–55.
[20] S. Mukherjee, S. Kalipatnapu, T.J. Pucadyil, A. Chattopadhyay, Monitoring the organization and dynamics of bovine hippocampal membranes utilizing differentially localized fluorescent membrane probes, Mol. Membr. Biol. 23 (2006) 430–441.
[21] A. Chattopadhyay, Exploring membrane organization and dynamics by the wavelength-selective fluorescence approach, Chem. Phys. Lipids 122 (2003) 3–17.
[22] S. Mukherjee, F.R. Maxfield, Membrane domains, Annu. Rev. Cell Dev. Biol. 20 (2004) 839–866.
[23] M. Hao, S. Mukherjee, F.R. Maxfield, Cholesterol depletion induces large scale domain segregation in living cell membranes, Proc. Natl. Acad. Sci. U. S. A. 98 (2001) 13072–13077.
[24] G. Krishnamoorthy, Ira, Fluorescence lifetime distribution in characterizing membrane heterogeneity, J. Fluoresc. 11 (2001) 247–253.
[25] Ira, G. Krishnamoorthy, Probing the link between proton transport and water content in lipid membranes, J. Phys. Chem., B 105 (2001) 1484–1488.
[26] P. Greenspan, S.D. Fowler, Spectrofluorometric studies of the lipid probe, Nile Red, J. Lipid Res. 26 (1985) 781–789.
[27] A.K. Dutta, K. Kamada, K. Ohta, Spectroscopic studies of Nile Red in organic solvents and polymers, J. Photochem. Photobiol., A 93 (1996) 57–64.
[28] N. Ghoneim, Photophysics of Nile Red in solution steady state spectroscopy, Spectrochim. Acta, A 56 (2000) 1003–1010.
[29] R.P. Haugland, Handbook of Fluorescent Probes and Research Chemicals, 6th ed. Molecular Probes Inc., Eugene, OR, USA, 1996.
[30] P.K. Smith, R.I. Krohn, G.T. Hermanson, A.K. Mallia, F.H. Gartner, M.D. Provenzano, E.K. Fujimoto, N.M. Goeke, B.J. Olson, D.C. Klenk, Measurement of protein using bicinchoninic acid, Anal. Biochem. 150 (1985) 76–85.
[31] T.J. Pucadyil, A. Chattopadhyay, Exploring detergent insolubility in bovine hippocampal membranes: a critical assessment of the requirement for cholesterol, Biochim. Biophys. Acta 1661 (2004) 9–17.
[32] D.M. Amundson, M. Zhou, Fluorometric method for the enzymatic determination of cholesterol, J. Biochem. Biophys. Methods 38 (1999) 43–52.
[33] E.G. Bligh, W.J. Dyer, A rapid method of total lipid extraction and purification, Can. J. Biochem. Physiol. 37 (1959) 911–917.
[34] C.W.F. McClare, An accurate and convenient organic phosphorus assay, Anal. Biochem. 39 (1971) 527–530.
[35] R. Koynova, M. Caffrey, Phases and phase transitions of the sphingolipids, Biochim. Biophys. Acta 1255 (1995) 213–236.
[36] D.E. Gueffroy, Buffers: A Guide for the Preparation and Use of Buffers in Biological Systems, Calbiochem-Behring, San Diego, CA, USA, 1983, p. 16.
[37] B. Valeur, Molecular Fluorescence Principles and Applications, Wiley-VCH, Weinheim, Germany, 2002.
[38] P.R. Bevington, Data Reduction and Error Analysis for the Physical Sciences, McGraw-Hill, New York, 1969.
[39] D.V. O'Connor, D. Phillips, Time-Correlated Single Photon Counting, Academic Press, London, 1984, pp. 180–189.
[40] R.A. Lampert, L.A. Chewter, D. Phillips, D.V. O'Connor, A.J. Roberts, S.R. Meech, Standards for nanosecond fluorescence decay time measurements, Anal. Chem. 55 (1983) 68–73.
[41] A. Grinvald, I.Z. Steinberg, On the analysis of fluorescence decay kinetics by the method of least-squares, Anal. Biochem. 59 (1974) 583–598.
[42] J.C. Brochon, Maximum entropy method of data analysis in time-resolved spectroscopy, Methods Enzymol. 240 (1994) 262–311.
[43] R. Swaminathan, G. Krishnamoorthy, N. Periasamy, Similarity of fluorescence lifetime distributions for single tryptophan proteins in the random coil state, Biophys. J. 67 (1994) 2013–2023.
[44] R. Swaminathan, N. Periasamy, Analysis of fluorescence decay by the maximum entropy method: influence of noise and analysis parameters on the width of the distribution of lifetimes, Proc. Indian Acad. Sci., Chem. Sci. 108 (1996) 39–49.
[45] S. Mukherjee, H. Raghuraman, A. Chattopadhyay, Membrane localization and dynamics of Nile Red: effect of cholesterol, Biochim. Biophys. Acta 1768 (2006) 59–66.

[46] W.K. Subczynski, A. Wisniewska, J.-J. Yin, J.S. Hyde, A. Kusumi, Hydrophobic barriers of lipid bilayer membranes formed by reduction of water penetration by alkyl chain unsaturation and cholesterol, Biochemistry 33 (1994) 7670–7681.
[47] M.M.G. Krishna, N. Periasamy, Fluorescence of organic dyes in lipid membranes: site of solubilization and effects of viscosity and refractive index on lifetimes, J. Fluoresc. 8 (1998) 81–91.
[48] G. Krishnamoorthy, A. Srivastava, Cell membrane dynamics seen through time-resolved fluorescence microscopy, Cell. Mol. Biol. Lett. 2 (1997) 145–163.
[49] P. Sharma, R. Varma, R.C. Sarasij, Ira, K. Gousset, G. Krishnamoorthy, M. Rao, S. Mayor, Nanoscale organization of multiple GPI-anchored proteins in living cell membranes, Cell 116 (2004) 577–589.
[50] K.J. Kinosita, S. Kawato, A. Ikegami, A theory of fluorescence polarization decay in membranes, Biophys. J. 20 (1977) 289–305.
[51] M. Murthy, J. Hamilton, R.S. Greiner, T. Moriguchi, N. Salem, H.-Y. Kim, Differential effects of n-3 fatty acid deficiency on phospholipid molecular species composition in the rat hippocampus, J. Lipid Res. 43 (2002) 611–617.
[52] L. Ulmann, V. Mimouni, S. Roux, R. Porsolt, J.-P. Poisson, Brain and hippocampus fatty acid composition in phospholipid classes of aged-relative cognitive deficit rats, Prostaglandins Leukot. Essent. Fat. Acids 64 (2001) 189–195.
[53] Z. Wen, H.-Y. Kim, Alterations in hippocampal phospholipid profile by prenatal exposure to ethanol, J. Neurochem. 89 (2004) 1368–1377.
[54] D.L. Sackett, J.R. Knutson, J. Wolff, Hydrophobic surfaces of tubulin probed by time-resolved and steady-state fluorescence of Nile Red, J. Biol. Chem. 265 (1990) 14899–14906.
[55] J.-R. Daban, M. Samsó, S. Bartolomé, Use of Nile Red as a fluorescent probe for the study of the hydrophobic properties of protein–sodium dodecyl complexes in solution, Anal. Biochem. 199 (1991) 162–168.
[56] F. Gao, E. Mei, M. Lim, R.M. Hochstrasser, Probing lipid vesicles by bimolecular association and dissociation trajectories of single molecules, J. Am. Chem. Soc. 128 (2006) 4814–4822.
[57] N.A. Pham, M.R. Gal, R.D. Bagshaw, A.J. Mohr, B. Chue, T. Richardson, J.W. Callahan, A comparative study of cytoplasmic granules imaged by the real-time microscope, Nile Red and Filipin in fibroblasts from patients with lipid storage diseases, J. Inherited Metab. Dis. 28 (2005) 991–1004.
[58] T. Parasassi, M.D. Stefano, M. Loiero, G. Ravagnan, E. Gratton, Cholesterol modifies water concentration and dynamics in phospholipid bilayers: a fluorescence study using laurdan probe, Biophys. J. 66 (1994) 763–768.
[59] R.B. Gennis, Biomembranes: Molecular Structure and Function, Springer-Verlag, New York, 1989.
[60] T.J. Pucadyil, A. Chattopadhyay, Effect of cholesterol on lateral diffusion of fluorescent lipid probes in native hippocampal membranes, Chem. Phys. Lipids 143 (2006) 11–21.
[61] A.G. Lee, Lipid–protein interactions in biological membranes: a structural perspective, Biochim. Biophys. Acta 1612 (2003) 1–40.
[62] T. Parasassi, M.D. Stefano, M. Loiero, G. Ravagnan, E. Gratton, Influence of cholesterol on phospholipid bilayers phase domains as detected by Laurdan fluorescence, Biophys. J. 66 (1994) 120–132.
[63] H.R. Waterham, R.J.A. Wanders, Biochemical and genetic aspects of 7-dehydrocholesterol reductase and Smith–Lemli–Opitz syndrome, Biochim. Biophys. Acta 1529 (2000) 340–356.
[64] T.N. Tulenko, K. Boeze-Battaglia, R.P. Mason, G.S. Tint, R.D. Steiner, W.E. Connor, E.F. Labelle, A membrane defect in the pathogenesis of the Smith–Lemli–Opitz syndrome, J. Lipid Res. 47 (2006) 134–143.